Stability and Strength of Transition-Metal Tetraborides and Triborides

R. F. Zhang,[1,2] D. Legut,[3,4] Z. J. Lin,[5,6,*] Y. S. Zhao,[5] H. K. Mao,[6] and S. Veprek[2]

[1]*Theoretical Division, Los Alamos National Laboratory, Los Alamos, New Mexico 87545, USA*
[2]*Department of Chemistry, Technical University Munich, Lichtenbergstrasse 4, D-85747 Garching, Germany*
[3]*Nanotechnology Centre, VSB-Technical University of Ostrava, CZ-708 33 Ostrava, Czech Republic*
[4]*Atomistic Modelling and Design of Materials, University of Leoben, A-8700 Leoben, Austria*
[5]*LANSCE–LC, Los Alamos National Laboratory, Los Alamos, New Mexico 87545, USA*
[6]*Geophysical Laboratory, Carnegie Institution of Washington, NW Washington, D.C. 20015, USA*

Using density functional theory, we show that the long-believed transition-metal tetraborides (TB$_4$) of tungsten and molybdenum are in fact triborides (TB$_3$). This finding is supported by thermodynamic, mechanical, and phonon instabilities of TB$_4$, and it challenges the previously proposed origin of superhardness of these compounds and the predictability of the generally used hardness model. Theoretical calculations for the newly identified stable TB$_3$ structure correctly reproduce their structural and mechanical properties, as well as the experimental x-ray diffraction pattern. However, the relatively low shear moduli and strengths suggest that TB$_3$ cannot be intrinsically stronger than c-BN. The origin of the lattice instability of TB$_3$ under large shear strain that occurs at the atomic level during plastic deformation can be attributed to valence charge depletion between boron and metal atoms, which enables easy sliding of boron layers between the metal ones.

Recent attempts to design new intrinsically superhard materials ($H \geq 40$ GPa) concentrated on the introduction of light elements forming strong bonds (B, C, N, and O) into transition metals (T) with high elastic moduli [1–5]. The suggested compounds include $5d$ transition-metal diborides (e.g., OsB$_2$ [4] and ReB$_2$ [5]) and nitrides such as PtN [6], IrN$_2$ [7], and η-Ta$_2$N$_3$ [8,9]. Although some of these materials have high elastic moduli [4,5], the experimentally determined load-invariant hardnesses are typically below 30 GPa. Osmium diboride possesses high zero-pressure elastic moduli but a low hardness due to the presence of Os-Os layers with weak metallic bonds [10]. Rhenium diboride was believed to be intrinsically superhard [5], but its load-invariant hardness is also less than 30 GPa because of electronic and structural instabilities of $5d$ electrons under finite shear strain [11]. Rhenium nitrides, recently synthesized by Friedrich *et al.* [12] under high pressure and temperature, have attracted much interest because of their large bulk modulus of about 400 GPa, which is higher than that of ReB$_2$ of 334–371 GPa [5,13]. However, our recent first-principles study showed that a combination of thermodynamic instability, relatively low shear moduli and strengths, and relatively soft polar Re-N bonds inherently limits their hardness [14]. These findings strongly challenge the general idea to design intrinsically superhard transition-metal diborides based only on their high elastic moduli [3–5].

Great effort has been recently devoted to the synthesis of tetraborides of transition metals by introducing more boron atoms to form a three-dimensional boron network with strong covalent bonds [15–17] because of their economically inexpensive constituents and relatively high hardness as well as the practically feasible synthetic conditions that do not require high pressure. Using the hardness models, Wang *et al.* [15] suggested that the transition-metal tetraborides, such as WB$_4$ and MoB$_4$, should be intrinsically superhard. Unfortunately, tungsten tetraboride has load-invariant hardness less than 30 GPa [16], as recently confirmed by Mohammadi *et al.* [17]. These results raise doubts regarding the predictability of that hardness model (see also [18], and the general stability issue will be unveiled below).

The stability of tetraborides was questioned by Zhang *et al.* [19]. Using the structural evolution method, they reported that MoB$_4$ in WB$_4$ structure cannot exist because of its high positive formation energy and the presence of imaginary phonon frequencies. More recently, similar thermodynamic instability was addressed for tungsten tetraborides by Liang, Yuan, and Zhang [20]. These researchers have shown that, while MoB$_4$ and WB$_4$ are unstable, MoB$_3$ and WB$_3$ with two-dimensional boron layers sandwiched between the transition metals are stable. These results raise several questions: (i) Are triborides with the two-dimensional network mechanically and dynamically stable? (ii) Does the simulated x-ray diffraction (XRD) pattern of the TB$_3$ reproduce the experimental data? (iii) Could the calculated ideal shear resistance of the triborides support their possible superhardness? In this Letter, we show that the WB$_4$ structure, albeit a three-dimensional covalent boron network, cannot exist due to its general thermodynamic, mechanical, and dynamic instabilities. Instead, the triborides should be experimentally

accessible because of their thermodynamic, mechanical, and dynamic stability and because of the agreement of the simulated XRD pattern with the experimental one. We further demonstrate for the first time that, in spite of its two-dimensional covalent boron network, $T\text{B}_3$ possesses a high strength comparable to those of ReB_2 and B_6O. However, because the ideal shear strengths for $T\text{B}_3$ are much lower than those of c-BN, their intrinsic hardness should be also lower; i.e., they cannot be superhard.

First-principles calculations were performed by using the VASP code [21] with the generalized-gradient approximation proposed by Perdew and Wang for the exchange-correlation functional. Details of stress-strain calculations can be found in Refs. [22,23]. Dynamical properties of both $T\text{B}_4$ and $T\text{B}_3$ were calculated within the harmonic approximation by using the direct method based on the forces calculated via the Hellmann-Feynman theorem. To confirm our results, we also used a linear response method based on perturbation theory as implemented in the recent version of the VASP code. The resulting phonon dispersion and density of states (DOS) were the same as that using the $2 \times 2 \times 2$ supercell method. The equilibrium structural parameters for $T\text{B}_4$ and $T\text{B}_3$ ($T = \text{W}$ and Mo) (space groups: $P6_3/mmc$) were obtained by full relaxation of both lattice constants and internal atomic coordination. The relaxed atomic positions for $T\text{B}_4$ yielded four inequivalent crystallographic sites [$T2c$ $(1/3, 2/3, 1/4)$, $T2b$ $(0, 0, 1/4)$, B $12i$ $(1/3, 0, 0)$, and B $4f$ $(1/3, 2/3, 0.615)$]. The relaxed structure for $T\text{B}_3$ can be regarded as the absence of four boron atoms at B $4f$ $(1/3, 2/3, 0.615)$ from the $T\text{B}_4$ structures, which are cross-linking the boron hexagonal layer [Figs. 1(a) and 1(b)]. The optimized lattice constants of the four borides ($a = 5.36$ Å, $c = 6.47$ Å for WB_4, $a = 5.21$ Å, $c = 6.86$ Å for MoB_4, $a = 5.20$ Å, $c = 6.34$ Å for WB_3, and $a = 5.21$ Å, $c = 6.31$ Å for MoB_3) are in good agreement with the previous values [17,20], thus confirming the reliability of the present calculations. In addition, the calculated lattice constants of WB_3 show a better agreement with the experimentally reported tungsten borides ($a = 5.16$ Å, $c = 6.33$ Å) than those of WB_4 [17].

The bond structures of WB_4 and WB_3 at equilibrium are shown in Figs. 1(a) and 1(b). $T\text{B}_4$ can be regarded as a three-dimensional boron network (intercalated between the transition metals), consisting of planar hexagonal boron rings and out-of-plane vertical B-B dimers, which connect the neighbor hexagonal boron layers. In comparison, WB_3 consists of the hexagonal boron layer intercalated between adjacent metal layers. The major difference between WB_4 and WB_3 is the absence of the cross-linking B-B dimers in the latter. The maps of the electron localization function (ELF) on the $(10\bar{1}0)$ planes for WB_4 and WB_3 are also shown in Figs. 1(c) and 1(d), respectively. A higher value of ELF corresponds to higher electron localization. As one can see from Fig. 1(c), the strong B-B covalent bonds between the B-B dimers in WB_4
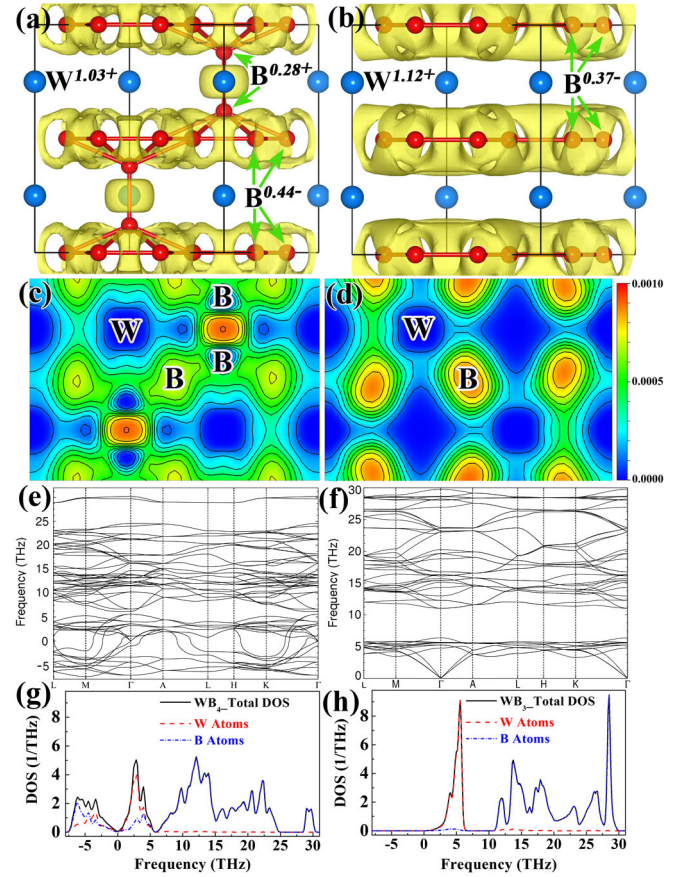

FIG. 1 (color online). Bond structures at equilibrium for (a) WB_4 and (b) WB_3. The isosurface maps of the ELF correspond to 0.0006 electrons/bohr^3; the large blue and small red spheres represent W and B atoms, respectively. Maps of the ELF on the $(10\bar{1}0)$ plane for (c) WB_4 and (d) WB_3. Calculated phonon dispersion curves for (e) WB_4 and (f) WB_3. The phonon density of states for (g) WB_4 and (h) WB_3. The numbers close to W and B atoms in (a) and (b) are the corresponding Bader charges.

indicate significant electron localization there. One might believe that such a three-dimensional cross-linking of the boron layers should stabilize and strengthen the structure. However, as shown below, the tetraborides are thermodynamically and dynamically instable.

To clarify the thermodynamic stability of $T\text{B}_4$ and $T\text{B}_3$, we calculated the formation energy with respect to the transition metal and boron (rhombohedral α-phase) based on the reactions $T + 4\text{B} = T\text{B}_4$ and $T + 3\text{B} = T\text{B}_3$, respectively. The resulting positive formation energies of WB_4 and MoB_4 are 0.41 and 0.28 eV/atom, respectively, suggesting that both tetraborides are thermodynamically unstable. On the contrary, the calculated formation energies of WB_3 and MoB_3 of -0.29 and -0.31 eV/atom, respectively, are negative, indicating that both triborides are thermodynamically stable. The distinct thermodynamic stability of tetraborides and triborides is in good agreement with previous work [19,20]. However, thermodynamic stability of the triborides does not guarantee their stability

TABLE I.   Single-crystal elastic constants c_{ij}, the Voigt bulk modulus B_V, shear modulus G_V, and ideal strength (minimum tensile strength σ_{min} and shear strength τ_{min}) of WB_3 (all in GPa) and MoB_3 calculated by first-principles methods. Previous theoretical results for ReB_2 [22], B_6O [24], c-BN [23], and diamond [24] are included for comparison.

Compound	Reference	c_{11}	c_{33}	c_{12}	c_{13}	c_{44}	B_V	G_V	σ_{min}	τ_{min}
WB_3	This study	639	470	106	169	262	293	245	$\sigma_{\langle 10\bar{1}0\rangle} = 43.3$	$\tau_{(0001)\langle 10\bar{1}0\rangle} = 37.7$
	[20]	656	479			277				
MoB_3	This study	602	427	106	160	241	276	226	$\sigma_{\langle 10\bar{1}0\rangle} = 37.7$	$\tau_{(0001)\langle 10\bar{1}0\rangle} = 34.1$
	[20]	602	420	106	166	247	276	222		
h-ReB_2	[22]	631	1015	158	134	257	348	274	$\sigma_{\langle \bar{1}2\bar{1}0\rangle} = 58.5$	$\tau_{(0001)\langle 10\bar{1}0\rangle} = 34.4$
h-B_6O	[24]	603	459	109	50	179	231	218	$\sigma_{\langle 10\bar{1}0\rangle} = 53.3$	$\tau_{(0001)\langle 10\bar{1}0\rangle} = 38.0$
c-BN	[23]	786		172		445	376	390	$\sigma_{\langle 111\rangle} = 55.3$	$\tau_{(111)\langle 11\bar{2}\rangle} = 58.3$
Diamond	[24]	1079		124		578	442	528	$\sigma_{\langle 111\rangle} = 82.3$	$\tau_{(111)\langle 11\bar{2}\rangle} = 86.8$

against transformation into another phase. Therefore, an analysis of elastic and dynamic stabilities is necessary.

To evaluate the mechanical stability of both triborides and tetraborides, we calculated their single-crystal elastic constants by using both the linear response method and the efficient strain-energy method [22]. The obtained "unrelaxed" elastic constants of WB_4 ($C_{11} = 379$ GPa, $C_{12} = 279$ GPa, $C_{13} = 226$ GPa, $C_{33} = 436$ GPa, and $C_{44} = 149$ GPa) are in good agreement with the previous calculations ($C_{11} = 389$ GPa, $C_{12} = 280$ GPa, $C_{13} = 224$ GPa, $C_{33} = 437$ GPa, and $C_{44} = 151$ GPa [15]). Interestingly, we found that the tetraboride structure may spontaneously transform to a lower energy state if an ionic relaxation is allowed along some shear distortion paths, such as $\varepsilon = (0, 0, 0, 0, 0, \delta)$ with $\Delta E/V_0 = \frac{1}{4}(C_{11} - C_{12})\delta^2$ and $\varepsilon = (0, 0, 0, 0, \delta, 0)$ with $\Delta E/V_0 = \frac{1}{2}C_{44}\delta^2$. To confirm this instability, we have introduced a small fluctuation of atomic position of boron atoms within basal planes; the structure cannot recover to the original symmetry. Such mechanical instability may be correlated to its large positive formation energy as discussed above and the dynamic instability as will be shown below. In contrast, both triborides are mechanically stable, and the elastic constants (ionic relaxation included) are listed in Table I for WB_3 and MoB_3.

Lattice dynamics was investigated for both TB_4 and TB_3. The dispersion relations of WB_4 and WB_3 are shown in Figs. 1(e) and 1(f) as examples. The phonon dispersion relation of WB_4 exhibits imaginary (negative) frequencies in several important directions showing its dynamic instability at $T = 0$ K. Indeed, the slope of the negative acoustic branch along the Γ-A high-symmetry direction in the vicinity of the Γ point corresponds to elastic constants of C_{44}. Similarly, for Γ-M and Γ-K the lower two branches are also negative close to the Γ point corresponding to negative C_{44} and $C_{66} = (C_{11} - C_{12})/2$. In contrast, the WB_3 phase is stable as there are no imaginary modes. The partial phonon DOSs of WB_3 and WB_4 [shown in Figs. 1(g) and 1(h)] indicate that the lower frequencies of the total DOS are dominated by lattice dynamics of heavy W atoms and higher frequencies by light B atoms. Moreover, there is a gap in phonon frequencies between ca. 6.5 and 10.5 THz in WB_3

that almost entirely separates higher frequencies dominated by vibrations of B and lower frequencies dominated by W atoms. On the other hand, in WB_4, there is an admixture of phonon states due to dynamics of B and W atoms and no gap in the phonon DOS at the lower frequencies, and some of the optical modes of B atoms are separated by a gap above 25 THz. The imaginary frequencies originate from both the lattice dynamics of W and B atoms.

The electronic DOSs were analyzed in order to obtain insights into the electronic origin of the different stabilities of the tetra- and triborides. The calculated electronic DOSs of WB_4, WB_3, MoB_4, and MoB_3 are shown in Fig. 2. Both tetraborides show metallic bonding because of the finite value of the DOS at the Fermi level (E_F), which originates mostly from d electrons of W or Mo and the p electrons of B. In the triborides, however, the DOS around E_F is lower than in tetraborides, and it shows a "splitting" into a pseudogap, thus underlying their stability. In the tetraborides, the pseudogap appears far below E_F, pointing to the electronic origin of their instability. Obviously, the B-B cross-linking dimers in the tetraborides weaken the bonds
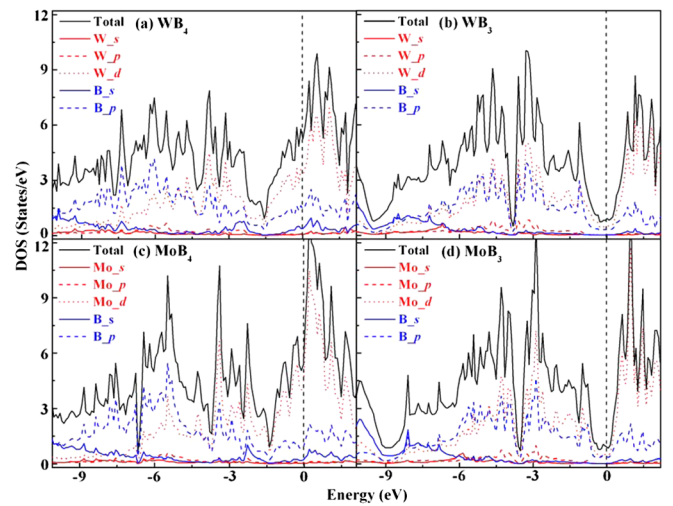

FIG. 2 (color online).   Total and partial electronic density of states of (a) WB_4, (b) WB_3, (c) MoB_4, and (d) MoB_3. The vertical dashed lines indicate the Fermi levels.

within the hexagonal boron layers and cause their less dense packing, because the nearest-neighbor B-B layer distances along the c axis of 3.168 Å for WB_3 and 3.154 Å for MoB_3 are shorter than those in tetraborides (3.235 Å for WB_4 and 3.429 Å for MoB_4). The Bader charge density analysis [25] shown in Fig. 1 further confirms the inhomogeneous charge transfer of the boron atoms at different crystallographic sites. Comparing the ELF of the tetraboride [Fig. 1(c)] with that of the triboride [Fig. 1(d)], one can understand that the weakening of the hexagonal boron layers in the former is due to a significant valence charge transfer to the cross-linking boron dimers.

In order to confirm the structure of the experimentally reported borides, we compared the simulated XRD patterns of triborides and tetraborides with the experimental one. Based on the similarity between tri- and tetraborides (the same space group $P6_3/mmc$), the triboride can be regarded as a boron-deficient tetraboride with an absence of B-B dimers. Therefore, a similar XRD pattern is expected for both. We calculated the XRD patterns for WB_4 and WB_3 and compared with the experimental one reported in Ref. [17]. The results are shown in Fig. 3. Obviously, all the simulated diffraction peaks for WB_3 are in excellent agreement with the experimental ones. In the simulated XRD pattern of WB_4, however, the intensity the (100), (200), (202), and (210) peaks is clearly higher than those shown in the experiment (almost invisible). These results

demonstrate that the tungsten borides prepared by Gu, Krauss, and Steurer [16] and Mohammadi *et al.* [17] are WB_3 rather than the long-believed WB_4. None of the lower energy structures of possible WB_4 has a better agreement with the experimental XRD pattern than WB_3.

The anisotropic ideal strength of the triborides was obtained from the calculated stress-strain relationships, which are shown in Figs. 4(a) and 4(b) and also summarized in Table I, and compared with those of hard ReB_2 [22] and superhard B_6O [24], c-BN [23], and diamond [24]. The minimum tensile strengths of WB_3 of 43.3 GPa and MoB_3 of 37.7 GPa are slightly lower than those of ReB_2 and B_6O, but the minimum shear strengths along the weakest $(0001)\langle 10\bar{1}0\rangle$ slip system are comparable to those of ReB_2 and B_6O. However, the ideal shear strengths of both triborides are lower than those of c-BN (58.3 GPa [23]), showing their lower shear resistance.

The structures of both WB_3 and MoB_3 before and after the shear instability were analyzed to understand their deformation mechanism. Both compounds show a similar instability mode. WB_3 is presented as an example in
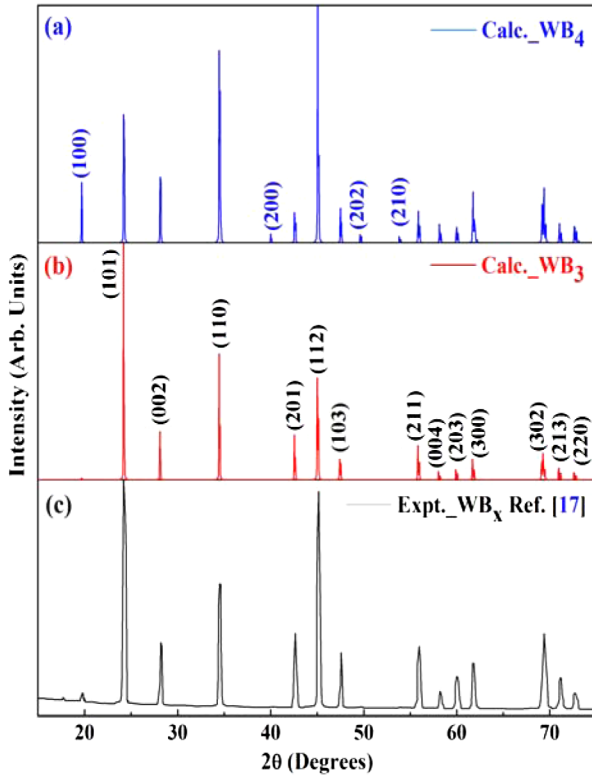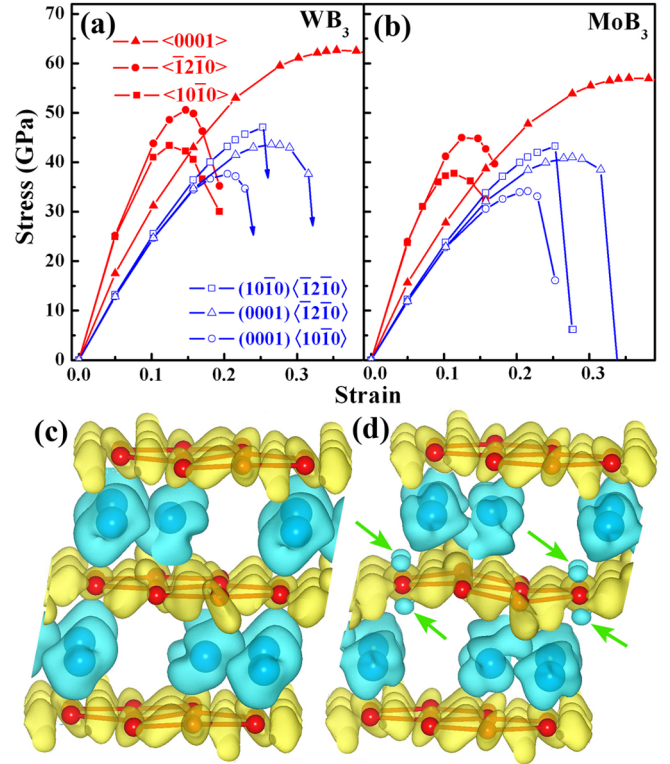
FIG. 4 (color online). Stress-strain relationships for (a) WB_3 and (b) MoB_3. Curves with solid symbols indicate tension deformations, and curves with open symbols denote shear deformations. The isosurfaces of deformed valence charge density difference of WB_3 at a shear strain of (c) $\gamma = 0.2044$ (before) and (d) $\gamma = 0.2531$ (after lattice instability) in the $(0001)\langle 10\bar{1}0\rangle$ slip system. The isosurfaces of valence charge density difference correspond to ± 0.016 electrons/bohr^3; large and small spheres represent tungsten and boron atoms, respectively. The arrows highlight the charge depletion states.

FIG. 3 (color online). Simulated XRD curves for (a) WB_4 and (b) WB_3. (c) Experimental XRD pattern for WB_x reproduced from Ref. [17].

Fig. 4, which shows the structure before and after lattice instability under the $(0001)\langle 10\bar{1}0\rangle$ shear deformation of about 20.4%. It can be seen that, after the lattice instability, the originally "flat" boron layers become wavy, and the valence charge density difference shows charge depletion between the boron and metal atoms, indicating breaking of the B-T bonds [see the arrows in Fig. 4(d)], which result in a sliding of the boron layers between the tungsten ones. This resembles the first shear instability in ReB$_2$ described in Ref. [11]. A more detailed comparison of the shear instabilities upon a larger shear, as described for ReB$_2$ in Ref. [11], is beyond the scope of the present study.

In summary, we carried out first-principles calculations to evaluate the thermodynamic, mechanical, and phonon stabilities of TB$_4$, which have been so far believed to be stable, in comparison with the TB$_3$. Electronic structure calculations reveal that the instability of tetraborides is associated with the weakening of the hexagonal boron layers due to strong localization of the p electron on the B-B dimers which are connecting adjacent boron layers. The stability issue of transition-metal tetraborides challenges the widely used "hardness model" (e.g., [15,26,27]), which incorrectly predicts them to be potentially superhard. The triborides are stable because such dimers are absent. The relatively low shear moduli and strength of transition-metal triborides indicate that they cannot be intrinsically superhard. An analysis of the deformed atomic and electronic structures reveals that the electronic instability is due to valence charge depletion between boron and metal atoms resulting in sliding of the boron layers between the tungsten ones, which limits their achievable strength.

---

*Corresponding author.
zjlin6@gmail.com

[1] D. M. Teter and R. J. Hemley, Science **271**, 53 (1996).

[2] S. Veprek, J. Vac. Sci. Technol. A **17**, 2401 (1999).

[3] R. B. Kaner, J. J. Gilman, and S. H. Tolbert, Science **308**, 1268 (2005).

[4] R. W. Cumberland, M. B. Weinberger, J. J. Gilman, S. M. Clark, S. H. Tolbert, and R. B. Kaner, J. Am. Chem. Soc. **127**, 7264 (2005).

[5] H. Y. Chung, M. B. Weinberger, J. B. Levine, A. Kavner, J. M. Yang, S. H. Tolbert, and R. B. Kaner, Science **316**, 436 (2007).

[6] E. Gregoryanz, C. Sanloup, M. Somayazulu, J. Badro, G. Fiquet, H. K. Mao, and R. J. Hemley, Nature Mater. **3**, 294 (2004).

[7] A. F. Young, C. Sanloup, E. Gregoryanz, S. Scandolo, R. J. Hemley, and H. K. Mao, Phys. Rev. Lett. **96**, 155501 (2006).

[8] A. Zerr, G. Miehe, J. W. Li, D. A. Dziewenko, V. K. Bulatov, H. Höfer, N. Bolfan-Casanova, M. Fialin, G. Brey, T. Watanabe, and M. Yoshimura, Adv. Funct. Mater. **19**, 2282 (2009).

[9] C. Jiang, Z. J. Lin, and Y. S. Zhao, Phys. Rev. Lett. **103**, 185501 (2009).

[10] J. Yang, H. Sun, and C. F. Chen, J. Am. Chem. Soc. **130**, 7200 (2008).

[11] R. F. Zhang, D. Legut, R. Niewa, A. S. Argon, and S. Veprek, Phys. Rev. B **82**, 104104 (2010).

[12] A. Friedrich, B. Winkler, L. Bayarjargal, W. Morgenroth, E. A. Juarez-Arellano, V. Milman, K. Refson, M. Kunz, and K. Chen, Phys. Rev. Lett. **105**, 085504 (2010).

[13] Y. J. Wang, J. Z. Zhang, L. L. Daemen, Z. J. Lin, Y. S. Zhao, and L. P. Wang, Phys. Rev. B **78**, 224106 (2008).

[14] R. F. Zhang, Z. J. Lin, H. K. Mao, and Y. S. Zhao, Phys. Rev. B **83**, 060101(R) (2011).

[15] M. Wang, Y. W. Li, T. Cui, Y. M. Ma, and G. T. Zou, Appl. Phys. Lett. **93**, 101905 (2008).

[16] Q. Gu, G. Krauss, and G. Steurer, Adv. Mater. **20**, 3620 (2008).

[17] R. Mohammadi, A. T. Lech, M. Xie, B. E. Eeaver, M. T. Yeung, S. H. Tolbert, and R. B. Kaner, Proc. Natl. Acad. Sci. U.S.A. **108**, 10 958 (2011).

[18] S. Veprek, A. S. Argon, and R. F. Zhang, Philos. Mag. **90**, 4101 (2010).

[19] M. G. Zhang, H. Wang, H. B. Wang, T. Cui, and Y. M. Ma, J. Phys. Chem. C **114**, 6722 (2010).

[20] Y. C. Liang, X. Yuan, and W. Q. Zhang, Phys. Rev. B **83**, 220102(R) (2011).

[21] G. Kresse and J. Furthmüller, Comput. Mater. Sci. **6**, 15 (1996).

[22] R. F. Zhang, S. Veprek, and A. S. Argon, Appl. Phys. Lett. **91**, 201914 (2007).

[23] R. F. Zhang, S. Veprek, and A. S. Argon, Phys. Rev. B **77**, 172103 (2008).

[24] R. F. Zhang, Z. J. Lin, Y. S. Zhao, and S. Veprek, Phys. Rev. B **83**, 092101 (2011).

[25] R. F. W. Bader, *Atoms in Molecules—A Quantum Theory* (Oxford University, New York, 1990).

[26] F. Gao, J. L. He, E. D. Wu, S. M. Liu, D. L. Yu, D. C. Li, S. Y. Zhang, and Y. J. Tian, Phys. Rev. Lett. **91**, 015502 (2003).

[27] A. Simunek and J. Vackar, Phys. Rev. Lett. **96**, 085501 (2006).